Dyes and Pigments 226 (2024) 112116

Contents lists available at ScienceDirect

Dyes and Pigments

journal homepage: www.elsevier.com/locate/dyepig

Synthesis and photophysical properties of *meta*-position-substituted triphenylmethyl-type radicals with non-conjugated donor/accepters

Ablikim Obolda [a,b,*], Wei Li [b], Zhaoze Ding [b], Fudong Ma [b], Mehrigul Abdulahat [b], Zhuoyang Hu [b], Jinquan Wang [a,**]

[a] College of Veterinary Medicine, Xinjiang Agricultural University, East Road No. 311, Urumqi, 830052, PR China
[b] College of Chemistry and Chemical Engineering, Xinjiang Agricultural University, East Road No. 311, Urumqi, 830052, PR China

ARTICLE INFO

Keywords:
Triphenylmethyl radical
Meta-substitution
Photostability
Proton-induced turn on fluorescence

ABSTRACT

In this study, we selectively modified a single *meta*-position of the tris-2,4,6-trichlorophenylmethyl (TTM) radical using non-conjugated donor (N,N-dimethyl group, –N(Me)$_2$) and acceptor (-Br, –NO$_2$) groups, resulting in three new TTM-type radicals: TTM-N(Me)$_2$, TTM-Br, and TTM-NO$_2$. Our findings indicated that, after the non-conjugated acceptors (-Br, -NO$_2$) directly attached to *meta*-position of TTM, there are no significant photophsical effect for TTM-Br, while TTM-NO$_2$ demonstrated a onefold increase in photostability and a threefold decrease in photoluminescent quantum yield (Φ_{PL}) compared to TTM. On the other hand, introducing a non-conjugated donor (-N(Me)$_2$) at the meta position of TTM, endowed TTM-N(Me)$_2$ with a remarkable 10,475-fold increase in photostability and activated proton-induced fluorescence. These unique properties could be attributed to the small energy gap between frontier orbitals and the proximity of energy levels between the singly occupied molecular orbital (SOMO) and the highest doubly occupied molecular orbital (HDMO), as revealed by quantum chemistry calculations and photophysical properties analysis. Our results offer valuable insights into meta-substituted TTM-type radicals and provide a new avenue for studying asymmetric *meta*-substituted TTM radicals.

1. Introduction

Due to the presence of an unpaired electron with distinctive electronic characteristics, such as an open-shell configuration, stable organic radicals have aroused significant attention for their potential applications across various fields [1]. These applications encompass chemical reactions [2], spintronics [3,4], molecular magnets [5,6], rechargeable batteries [7,8], photodynamic therapy [9], and organic field-effect transistors (OFETs) [10]. Notably, recent research has placed a substantial focus on stable luminescent radicals due to t the absence of quenching via intersystem crossing and absence of precious heavy metal effects. Consequently, internal quantum efficiency (IQE) in emissive radical-based organic light-emitting diodes (OLEDs) has reached up to 100% [11–14].

Within the realm of stable luminescent organic radicals, the most extensively studied family comprises derivatives of triarylmethyl radicals, such as perchlorotriphenylmethyl (PTM) [15], tris-2,4,6-trichlorophenylmethyl (TTM) [16], biphenyl-type triarylmethyl (BTM) (PyBTM) radicals [17–19], and other triarylmethyl-type radicals [20–22]. The chlorine atoms positioned at the *ortho* and *para* positions of the benzene ring provide effective shielding, preventing cyclization or dimerization of these triarylmethyl radicals. This stability is maintained at ambient temperature, even in the presence of oxygen. Recent research by Juliá, Li, Nishihara, and other scientists has demonstrated that rational molecular design can significantly enhance the photophysical properties of triarylmethyl-type radicals, including stability, photoluminescent quantum yield (Φ_{PL}), and sensitivity to solvents [23–25]. Earlier studies have shown that the stability and physical properties of PTM and TTM are similar, with the chlorine at the meta-position of PTM playing a less significant role. Conversely, the perchlorinated features of PTM contribute to its greater chemical inertness but unsuitability for optional chemical modification[26]. In this context, TTM-type radicals emerge as promising candidates for chemical modification to enhance their photophysical properties.

* Corresponding author. College of Veterinary Medicine, Xinjiang Agricultural University, East Road No. 311, Urumqi, 830052, PR China.
** Corresponding author.
E-mail address: aobolda@126.com (A. Obolda).

https://doi.org/10.1016/j.dyepig.2024.112116
Received 15 October 2023; Received in revised form 21 March 2024; Accepted 25 March 2024
Available online 29 March 2024

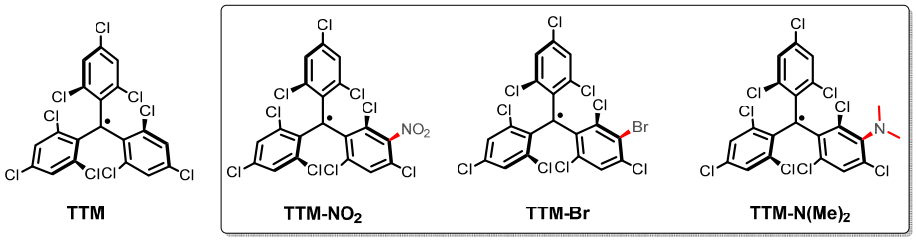

Scheme 1. molecular structure of TTM, TTM-NO_2, TTM-Br, TTM-N $(Me)_2$.

To date, the majority of chemical modification methods have been limited to the *para*-position of TTM, with little exploration of the *meta* or *ortho*-positions. Recent reports by Hattori and colleagues have demonstrated that introducing aromatic donors or acceptors at the *meta*-positions of the two phenyl rings in BTM-type radicals can lead to a significant increase in photostability and fluorescence quantum yield [27,28]. However, to the best of our knowledge, there have been no previous reports on the selective modification of the *meta*-position of TTM with non-conjugated donors or acceptors, especially with a non-conjugated donor directly attached to TTM. We hypothesize that the close proximity of a non-conjugated donor to TTM could enhance the interaction between the donor and the radical center, resulting in unique photophysical properties.

In our study, we selectively modified the sole *meta*-position of TTM with different non-conjugated donors/acceptors (-$N(Me)_2$, -Br, and –NO_2) to produce radicals: (N,N′-dimethyl phenyl) bis(2,4,6-trichlorophenyl)methyl (TTM-$N(Me)_2$), (3-bromo-2,4,6-trichlorophenyl)bis(2,4,6-trichlorophenyl)methyl (TTM-Br), and (3-nitro-2,4,6-trichlorophenyl)bis(2,4,6-trichlorophenyl)methyl (TTM-NO_2) (Scheme 1). Photophysical analysis and DFT calculations of these radicals revealed that the substitution of donor units (-Br and –NO_2) had minimal impact on the photophysical properties of radicals TTM-Br and TTM-NO_2. In contrast, the photostability of TTM-$N(Me)_2$ significantly increased, and it exhibited fluorescence upon protonation. Furthermore, the successful synthesis of bromide TTM-Br opens up new avenues for studying asymmetric meta-substituted TTM radicals.

2. Experimental section

2.1. General information

All chemicals were purchased from Tansoole Chemicals and commercial suppliers and used as received unless stated otherwise. THF and $CHCl_3$ were distilled with standard method before use.

The ^{1}H NMR spectra were recorded with a Bruker AVANCZ 500 spectrometer at 400 or 500 MHz, using deuterated chloroform (CD_3Cl) as solvent at 298 K. The mass spectra of the radical precursor and radical were recorded on MALDI-TOF (Brucker Auto) mass spectrometer for low resolution and LCMS-IT-TOF (Shimadzu) for high resolution. Elemental analyses were recorded with a Elementar Various EL Cube. Fourier transform Infrared (FT-IR) spectra were recorded using a Bruker VERTEX 70. Ultraviolet–visible (UV–vis) absorption spectra of the radicals were recorded on a Shimadzu UV-2600 spectrophotometer. Fluorescence spectra of the radicals were performed using Agilent G9800A spectrophotometer. The fluorescence decay spectra were recorded on an Edinburgh fluorescence spectrometer (FLS980), and the lifetime of the excited states was measured by the time-correlated single photon counting method under the excitation of a laser (378 nm). Relative fluorescence quantum yields are determined for cyclohexane solutions of the radicals upon excitation at 375 nm, using TTM as a standard. EPR spectra were recorded on a Bruker ELEXSYSII E500 CW-EPR spectrometer at ambient atmosphere in dichloromethane. Thermal gravimetric analyses (TGA) were performed with a SHIMADZU DTG-60 thermal analyzer at heating rate of 10 °C/min under nitrogen protection. Column

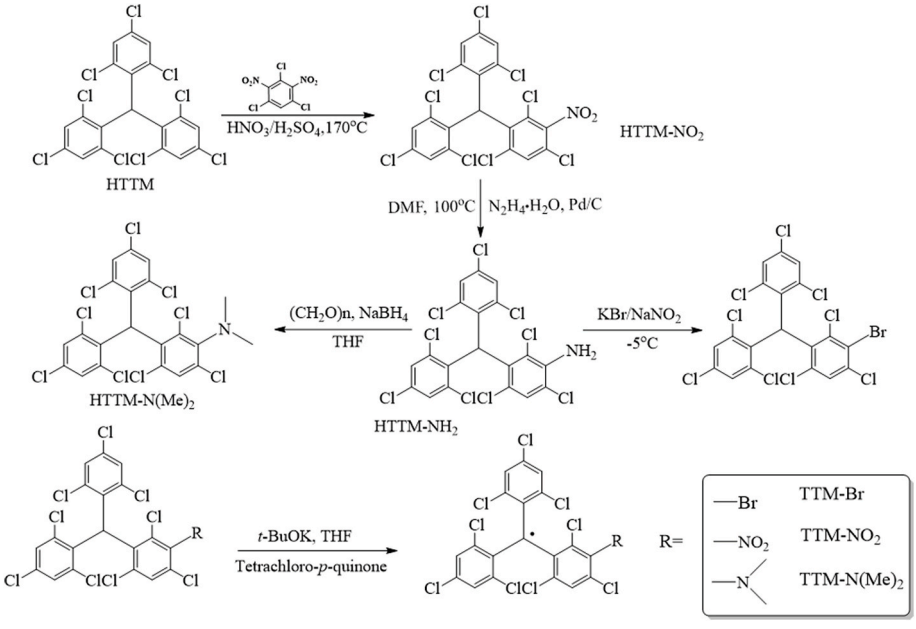

Scheme 2. Synthetic procedure of the radical TTM-NO_2, TTM-Br and TTM-$N(Me)_2$ and its precursor.

chromatography was performed with silica gel (300–400 mesh). Photostability of the radicals was achieved by measuring decay of fluorescence spectra or 375 nm-centered UV–vis spectra at the same condition.

2.2. Synthesis and characterization

The synthetic routes and molecule structures of these novel radicals were depicted in Scheme 2. As shown, the radical TTM-Br, TTM-NO_2 and TTM-N$(Me)_2$ were achieved from its precursor via deprotonation and oxidation processes. Detailed synthetic procedure of the radicals and its precursor HTTM-Br, HTTM-NO_2 and HTTM-N$(Me)_2$ were as follow.

Synthesis of (3-nitro-2,4,6-trichlorophenyl)bis(2,4,6-trichlorophenyl) methane (HTTM-NO_2). 2.0 g (3.6 mmol) HTTM was added to a 100 mL two-neck glass reactor and 2.0 g (7.4 mmol) 1,3,5-trichloro-2,4-dinitrobenzene was added to the reaction as solvent, and heated to 170 °C, after reaction mixture was melted, 3 mL (56.3 mmol) concentrated sulfuric acid and 2 mL (44.8 mmol) concentrated nitric acid were added slowly and reacted for 2 h. After reaction was completed, the reaction mixture was cooled to room temperature, neutralized with saturated Na_2CO_3 and extracted with dichloromethane. The collected organic layer was dried with anhydrous sodium sulfate and crude product was separated by column chromatography (eluent: petroleum ether/dichloromethane (5/1), obtained 0.65 g white solid of HTTM-NO_2 (30%). Analyzing the ^{1}H NMR spectrum of HTTM-NO_2, we can find that signals at the 7.47–7.24 ppm attributed to the 5 hydrogens from three phenyl rings. However, it should be noted that signal of the central methylene unit (at 6.70 ppm) was divided into two singlet peaks due to the axial chirality (please see from supporting information section). Melting point = 235–236 °C. MALDI-TOF MS (mass *m/z*):598.17[M − 2]$^+$; ^{1}H NMR (400 MHz, $CDCl_3$, 25 °C, TMS) δ(ppm) 7.47 (d, J = 51.9 Hz, 1H), 7.39–7.34 (m, 2H), 7.24 (s, 2H), 6.70 (d, 1H). ^{13}C NMR (101 MHz, $CDCl_3$) δ(ppm) 139.07, 137.93, 137.88, 137.78, 137.58, 137.52, 137.06, 136.99, 136.98, 136.94, 136.35, 136.32, 134.47, 134.40, 134.38, 134.32, 132.81, 132.71, 132.65, 132.55, 131.09, 131.05, 130.25, 130.24, 130.15, 130.08, 129.63, 129.58, 129.51, 128.67, 128.53, 128.50, 128.24, 125.32, 125.21, 50.19, 50.17, 50.16, 50.12.

Synthesis of (3-amino-2,4,6-trichlorophenyl)bis(2,4,6-trichlorophenyl) methane (HTTM-NH_2). A mixture of 1.0 g (1.7 mmol) HTTM-NO_2, 0.05 g Pd/C (palladium on activated charcoal) and hydrazine monohydrate 2 mL (30.0 mmol) and 10 ml of DMF was stirred at 100 °C for 12 h under nitrogen atmosphere. After reaction was completed, the Pd/C was separated by filtration. The filtrate was concentrated by rotary evaporator under reduced pressure. The crude product was purified by column chromatography (eluent: petroleum ether/dichloromethane, 5/1) to afford 0.53 g white solid of HTTM-NH_2 (55%). ^{1}H NMR data showed that signals at 7.38–7.22 ppm are attributed to 5 hydrogens from three phenyl rings, the signal from the central methylene unit (at 6.68 ppm) was divided into two singlet peaks due to the axial chirality, and signal of NH_2 appeared at 4.48 ppm (please see from supporting information). MALDI-TOF MS (mass *m/z*):569.36[M − 1]$^+$; ^{1}H NMR (500 MHz, $CDCl_3$) δ(ppm) 7.38 (s, 2H), 7.29 (d, J = 24.9 Hz, 2H), 7.22 (d, J = 27.2 Hz, 1H), 6.68 (d, 1H), 4.50 (s, 2H).

Synthesis of (3-bromo-2,4,6-trichlorophenyl)bis(2,4,6-trichlorophenyl) methane (HTTM-Br). The mixture of 0.5 g (0.88 mmol) HTTM-NH_2 and 5 mL hydrobromic acid was cooled to -5—0 °C and 0.18 g(2.6 mmol) sodium nitrite solution was added slowly, and reacted for 0.5 h, after then, 0.31 g (2.6 mmol) potassium bromide solution was added dropwise. The reaction was carried out until the precipitate was formation. After reaction was completed, the reaction mixture was extracted by dichloromethane; the organic layer was collected and dried with anhydrous sodium sulfate. The crude product was separated by column chromatography (eluent: petroleum ether), obtained 0.37 g (67%) white solid of HTTM-Br. ^{1}H NMR data showed that signals at 7.48–7.22 ppm attributed to 5 hydrogens at three phenyl rings, the signal from the central methylene unit (at 6.69 ppm) was divided into two singlet peaks due to the axial chirality (please see from supporting information). Melting point = 201–203 °C.MALDI-TOF MS (mass *m/z*):635.63[M]$^+$; ^{1}H NMR (400 MHz, $CDCl_3$) δ(ppm) δ 7.48–7.32 (m, 3H), 7.22 (dd, J = 4.4, 2.1 Hz, 2H), 6.69 (d, 1H). ^{13}C NMR (101 MHz, $CDCl_3$) δ(ppm) 139.03, 138.04, 137.95, 137.89, 137.77, 137.72, 137.10, 137.06, 137.04, 136.87, 136.31, 135.75, 135.60, 135.54, 135.41, 135.35, 133.92, 133.87, 133.80, 133.76, 133.64, 133.62, 133.56, 130.53, 130.49, 130.03, 129.98, 129.01, 128.97, 128.49, 128.42, 124.88, 123.31, 51.49, 51.47, 51.06, 51.04, 49.80, 49.78.

Synthesis of (N,N′-dimethyl phenyl) bis(2,4,6-trichlorophenyl)methane (HTTM-N$(Me)_2$). The mixture of 0.60 g paraformaldehyde and 10 mL 60% of sulfuric acid was stirred at 100 °C for 1 h and cooled to room temperature for next step use. To another 50 mL round-bottom flask, 0.30 g (0.53 mmol) HTTM-NH_2, 0.50 g (13.2 mmol) sodium borohydride ($NaBH_4$) was added and dissolved in 15 mL THF. After then, the prepared mixture of paraformaldehyde in sulfuric acid was added to the reaction, the reaction was stirred at room temperature for 0.5 h. After the reaction was neutralized and extracted with dichloromethane, the organic layer was dried with anhydrous sodium sulfate and crude product was separated by column chromatography (eluent: petroleum ether/dichloromethane, 5/1), obtained 0.23 g (72%) white solid of HTTM-N$(Me)_2$. ^{1}H NMR data of TTM-N$(Me)_2$ showed that signals at 7.33–7.21 ppm are attributed to 5 hydrogens at three phenyl rings, the signal from the central methylene unit (at 6.67 ppm) was divided into two singlet peaks due to the axial chirality, and signals of N$(Me)_2$ were appeared at 2.79 ppm (please see from supporting information). Melting point = 73–75 °C. HRMS (mass *m/z*):597.54[M]$^+$; ^{1}H NMR (400 MHz, $CDCl_3$) δ 7.33 (t, J = 3.1 Hz, 2H), 7.21 (q, J = 3.0 Hz, 3H), 6.67 (d, 1H), 2.79 (d, J = 22.6 Hz, 6H). ^{13}C NMR (101 MHz, $CDCl_3$) δ(ppm) 146.60, 145.79, 140.13, 138.45, 137.99, 137.90, 137.80, 137.14, 137.05, 136.89, 134.97, 134.80, 134.62, 134.49, 134.45, 134.20, 134.16, 133.59, 133.52, 133.43, 132.94, 132.20, 130.75, 130.74, 130.01, 129.96, 129.88, 129.20, 129.17, 128.36, 50.77, 50.75, 50.67, 50.65, 42.01, 41.89, 41.85, 29.69.

2.2.1. Synthesis of radical TTM-NO_2, TTM-Br and TTM-N$(Me)_2$

In nitrogen atmosphere and dark condition, related radical precursors (50 mmol, HTTM-NO_2, HTTM-Br or HTTM-N$(Me)_2$) were added to 100 mL round-bottom flask and dissolved in 30 mL freshly distilled THF, after then (250 mmol) potassium tert-butoxide (*t*-BuOK) was added to the reaction. The reaction mixture was stirred at room temperature for 5 h, and then (150 mmol) tetrachloro-*p*-quinone was added and stirred for 1 h. After reaction was completed, the crude product was separated by column chromatography (eluent: petroleum ether/dichloromethane, 5/1), finally obtained deep red solid TTM-NO_2 (61%) and TTM-Br (67%), and dark brown solid TTM-N$(Me)_2$ (45%). Characterization of TTM-Br: ESI-HRMS (*m/z*): calcd. for $C_{19}H_5BrCl_9$: [M]$^+$ 626.6766, found 626.6960; Anal. calcd. (%) For $C_{19}H_5BrCl_9$: C 36.10, H 0.80; Found: C 37.22, H 0.69. FT-IR (KBr, ν.cm^{-1}): 3090 (Ar, C–H), 1627, 1552, 1519(Ar, C═C), 565(C–Br). Characterization of TTM-NO_2: ESI-HRMS (*m/z*): calcd. for $C_{19}H_5Cl_9NO_2$: [M]$^+$ 593.7512, found 593.7336; Anal. calcd. (%) For $C_{19}H_5Cl_9NO_2$: C 38.14, H 0.84, N 2.34; Found: C 38.43, H 0.66, N 2.32. FT-IR (KBr, ν.cm^{-1}): 3079 (Ar, C–H), 1547(ν_{as} = NO_2), 1349 (ν_s = NO_2). Characterization of TTM-N$(Me)_2$: ESI-HRMS (*m/z*): calcd. for $C_{21}H_{11}Cl_9N$: [M+H]$^+$ 592.8161, found 592.8156; Anal. calcd. (%) For $C_{21}H_{11}Cl_9N$: C 42.29, H 1.86, N 2.35; Found: C 43.57, H 1.79, N 2.36. FT-IR (KBr, ν.cm^{-1}): 3071 (Ar, C–H), 2924, 2854 (CH_3), 1669, 1552, 1518 (Ar, C═C), 1366 (CH_3).

3. Result and discussion

3.1. Photophysical properties

The UV–vis absorption spectra of TTM-Br, TTM-NO_2, and TTM-N$(Me)_2$ were recorded in cyclohexane and compared to those of TTM. All the radicals exhibited two distinctive absorption features, with a pronounced peak at approximately 370 nm and a weaker absorption band

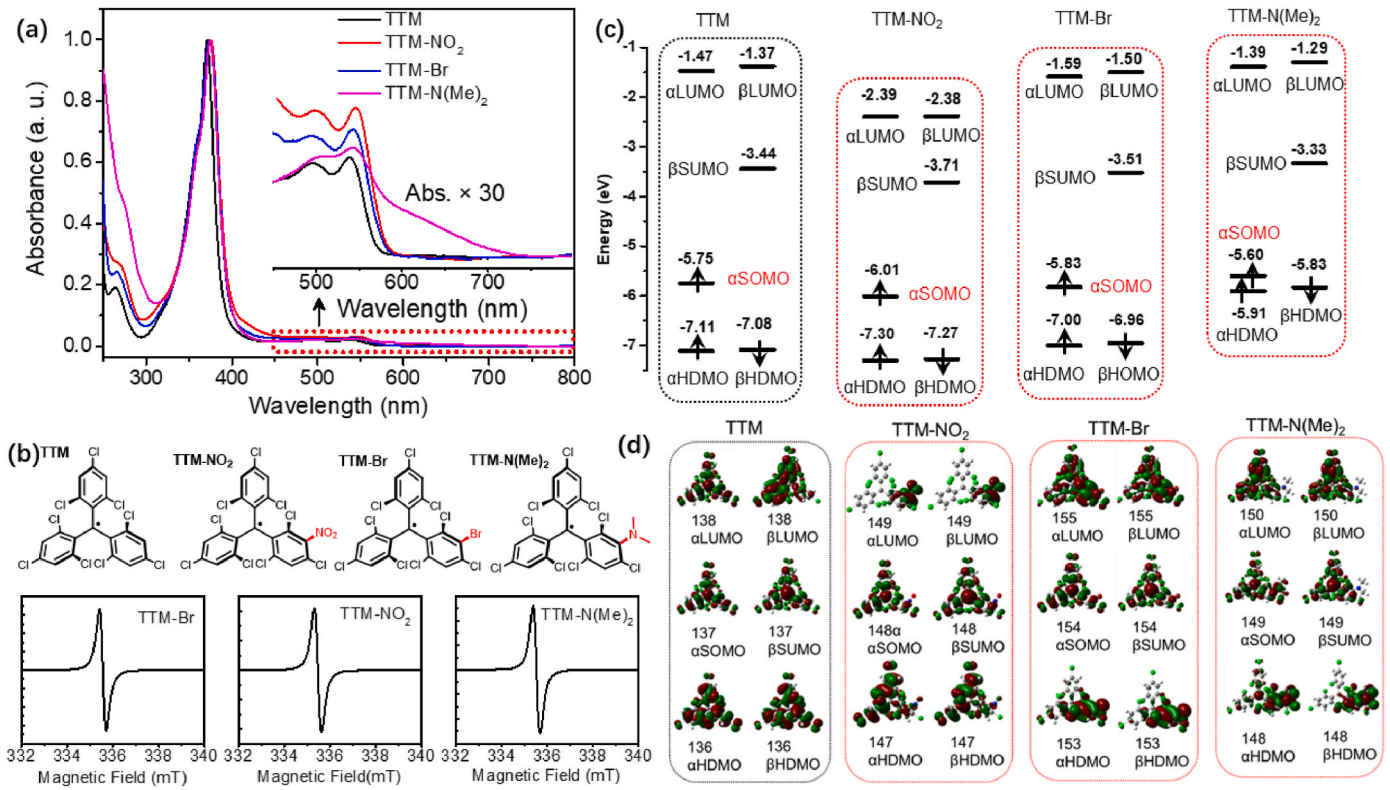

Fig. 1. (a) Absorption of TTM-NO_2, TTM-Br, TTM-N $(Me)_2$ and TTM in cyclohexane at room temperature. Enlarged portion of the absorption spectra (30-fold) are shown from λ = 450 nm–800 nm. (b) Molecular structures and EPR spectra of TTM-NO_2, TTM-Br and TTM-N $(Me)_2$ in CH_2Cl_2 at room temperature. (c) Energies and (d) molecular orbitals of TTM, TTM-NO_2, TTM-Br and TTM-N$(Me)_2$ at the UB3LYP/6-31G (d, p) level.

extending beyond 430 nm. The 370 nm-centered short-wavelength absorptions of TTM-Br, TTM-NO_2, and TTM-N$(Me)_2$ exhibited a slight redshift (1–3 nm) in comparison to TTM, attributable to the auxochromic effect. As illustrated in the inset of Fig. 1a, when compared to TTM, the intensities of the long-wavelength absorptions at around 540 nm in TTM-Br, TTM-NO_2, and TTM-N$(Me)_2$ increased to varying degrees. Intriguingly, TTM-N$(Me)_2$ displayed a weak longer-wavelength absorption that extended beyond λ = 725 nm, which is considerably longer than that of TTM-Br and TTM-NO_2. This phenomenon is likely attributed to the strong donor characteristics of the –N$(Me)_2$ unit. Electron spin resonance (EPR) spectroscopy of TTM-Br, TTM-NO_2, and TTM-N$(Me)_2$ in CH_2Cl_2 at room temperature (Fig. 1a) revealed EPR signals with g-factors (g) ranging from 2.0038 to 2.0040, indicative of unpaired carbon-centered radicals.

To gain a deeper understanding of the electronic structures and frontier orbitals of the radicals, we conducted density functional theory (DFT) and time-dependent DFT (TD-DFT) calculations using Gaussian09 software at the UB3LYP/6-31G (d, p) level. As depicted in Fig. 1c and d, the calculated singly occupied molecular orbital (αSOMO) levels for the TTM-Br, TTM-NO_2, and TTM-N$(Me)_2$ radicals were found to be −6.01, −5.83, and −5.60 eV, with βSOMO energies of −3.71, −3.51, and −3.33 eV, respectively. It was observed that the substituents, -Br and –NO_2, led to a partial lowering of the energy levels of αSOMO and singly unoccupied molecular orbital (βSUMO) in TTM-NO_2 and TTM-Br, compared to TTM. Conversely, the frontier energy levels (αSOMO and βSUMO) of the TTM-N$(Me)_2$ radical were raised after the substitution with –N$(Me)_2$. These outcomes are consistent with the distinct donor or acceptor properties of the substituents. Intriguingly, the introduction of the –N$(Me)_2$ group into TTM significantly elevated the levels of the highest doubly occupied molecular orbital (HDMO), possibly accounting for the shift of lower energy absorption in the TTM-N$(Me)_2$ radical to 725 nm. Furthermore, the TD-DFT calculation result of the radical TTM-N$(Me)_2$ showed that the very weak charge transfer (CT) sate absorption comes from the electron transition of βHDMO→βSUMO, which is

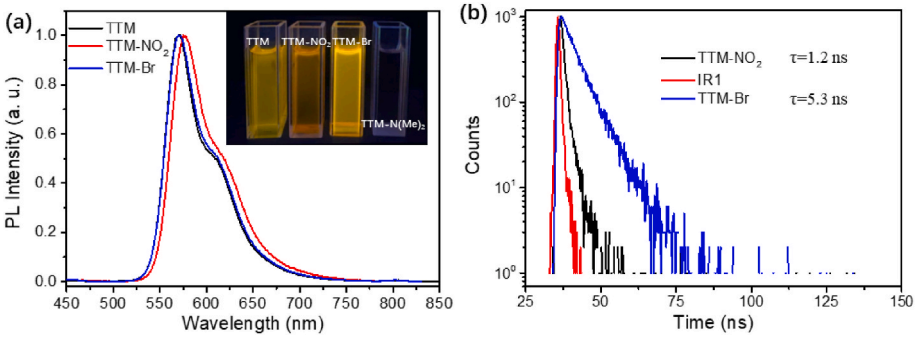

Fig. 2. (a) PL emission spectra of TTM TTM-NO_2 and TTM-Br (inset shows the photographs of the TTM TTM-NO_2 and TTM-Br in cyclohexane solution under the irradiation with a 365 nm UV lamp at ambient temperature; (b) PL decay of TTM-NO_2 and TTM-Br in cyclohexane solution at room temperature.

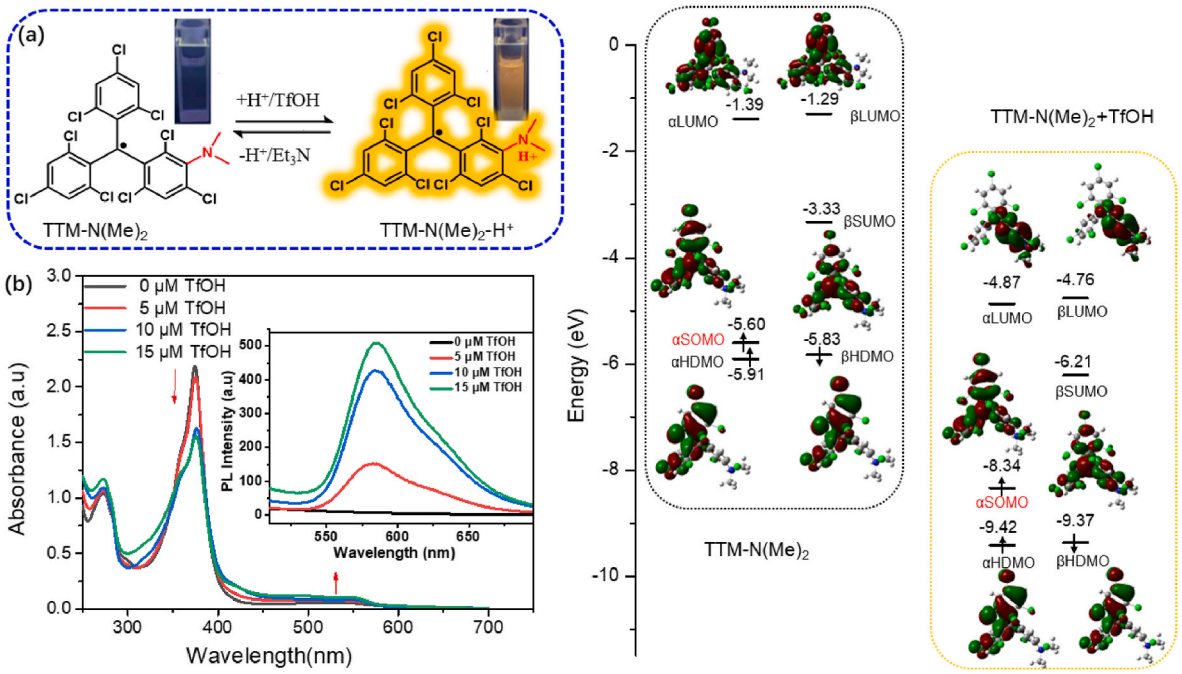

Fig. 3. (a) Molecular structures of the radical TTM-N(Me)$_2$ and its protonated state TTM-N(Me)$_2$+H and their photographs in cyclohexane under 365 nm UV lamp irradiation; (b) UV–vis spectra of TTM-N(Me)$_2$ (10^{-4} mol/L) with different concentration TfOH; inset shows corresponding PL spectra of protonated TTM-N(Me)$_2$ (TTM-N(Me)$_2$+H); (c) Energies and molecular orbitals of TTM-N(Me)$_2$ and its protonated state (TTM-N(Me)$_2$+H).

common for donor-acceptor (A-D)-type radicals. Due to the different properties of these substitutions, the shapes of the frontier orbitals in the radicals vary. Nevertheless, the shapes of the SOMO and SUMO closely resemble those of TTM and are predominantly located on the triarylmethyl unit. For the TTM-Br and TTM-N(Me)$_2$ radicals, the majority of the electron density in the HDMOs is situated on -Br, –N(Me)$_2$, and the attached phenyl rings. TD-DFT results indicated that the strong absorptions centered at 370 nm in the radicals TTM-Br, TTM-NO$_2$, and TTM-N(Me)$_2$ could be attributed to electron transitions from αSOMO to αLUMO or higher αLUMO, a well-known feature of triphenylmethyl-type radicals [11,29,30].

Emission spectra of the radicals were recorded in cyclohexane and compared to TTM. As seen in Fig. 2a, the emission bands for TTM-Br and TTM-NO$_2$ were observed at 571 nm and 577 nm when excited at 370 nm. The emission peak of TTM-Br remained unchanged, while that of TTM-NO$_2$ exhibited a slight redshift of 6 nm compared to TTM (571 nm). However, the TTM-N(Me)$_2$ radical did not exhibit fluorescence in common organic solvents, this could be synergistic effects from the several factors, such as very weak electronic coupling between the first ground state and excited state, energy dissipation from the flexible unit –N(Me)$_2$ and small energy gap, as confirmed by TD-DFT calculation and the absorption spectrum [31,32]. The photoluminescence quantum efficiency (PL) Φ_{PL} for TTM-Br and TTM-NO$_2$ in cyclohexane was measured to be 2.9% and 0.8%, compared to that of TTM (Φ_{PL} = 3.0%) [33]. Due to the well-known quenching effect of the nitro group, the TTM-NO$_2$ radical displayed lower Φ_{PL} than TTM, while TTM-Br exhibited a Φ_{PL} nearly identical to that of TTM, indicating that the introduction of the bromine atom did not significantly affect the Φ_{PL} of the radical. We also conducted PL transient decay measurements in cyclohexane, toluene, and chloroform (Fig. 2 and S1), which revealed that the PL transient decay of TTM-Br in cyclohexane was 5.3 ns, closely resembling that of TTM (5.5 ns). Conversely, the lifetime of TTM-NO$_2$ was hardly detectable, only 1.2 ns.

3.2. Protonation–deprotonation properties of TTM-N(Me)$_2$

What particularly captures our attention is the non-emissive nature of the radical TTM-N(Me)$_2$ in both solvents and solid states. We hypothesize that a close-range, robust electronic interaction between the radical center and a pair of unpaired electrons from the –N(Me)$_2$ unit might be responsible for the minimal energy gap in TTM-N(Me)$_2$, thereby resulting in the absence of fluorescence. To confirm this hypothesis, we conducted a protonation-deprotonation reaction and observed a striking transformation in the non-emissive radical TTM-N(Me)$_2$. Upon the addition of trifluoromethanesulfonic acid (TfOH), strong emission was induced, which reverted to a neutralized state following base titration with triethylamine (Et$_3$N).

As shown in Fig. 3, the concentration of TfOH displayed a direct impact. The short-wavelength absorption peaks of TTM-N(Me)$_2$ (10^{-4} mol/L) in cyclohexane (centered at 375 nm) decreased as TfOH concentration increased, while the long-wavelength absorption bands, which corresponds to intramolecular charge transfer (ICT), was slightly increased and bathochromically shifted. The emission peaks at 585 nm for TTM-N(Me)$_2$ gradually intensified upon the addition of TfOH, reaching their maximum at 15 μM (The absorption spectra upon further addition of TfOH was given in the supporting information S2). Our hypothesis is that the protonation process disrupts the electronic interaction between the radical center and unpaired electrons from the –N(Me)$_2$ unit, simultaneously lowering the HDMO level of TTM-N(Me)$_2$, leading to the activation of fluorescence upon protonation.

To substantiate our conjecture, we performed DFT and TD-DFT calculations for protonated TTM-N(Me)$_2$ (please refer to the supporting information). As anticipated, protonation resulted in the stabilization of the –N(Me)$_2$ unit and a decrease in electron density. This, in turn, led to a reduction in the energy levels of the frontier orbitals of TTM-N(Me)$_2$ and an expansion of the energy gaps between αHDMO-αSOMO and βHDMO-βSUMO. As illustrated in Fig. 3c, the electron cloud density of the HDMO orbital of TTM-N(Me)$_2$ predominantly resided on the –N(Me)$_2$ unit and the phenyl rings attached to –N(Me)$_2$. Conversely, following protonation, most of the electron cloud densities of HDMOs shifted to the other two phenyl rings. Furthermore, the corresponding oscillator strength of the radical TTM-N(Me)$_2$ from the ground state (D_0) to the first excited state (D_1) increased from f = 0.0090 to f = 0.0418 after protonation. This enhanced transition probability is indicative of its

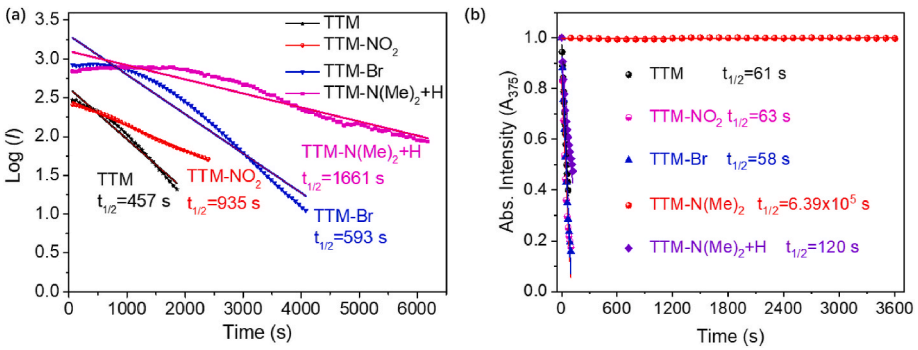

Fig. 4. (a) Comparison of fluorescence decay of TTM, TTM-NO_2, TTM-Br and protonated TTM-N$(Me)_2$(TTM-N$(Me)_2$+H) in cyclohexane at the same instrument settings; (b) Comparison of absorbance (at 375 nm) decay of TTM and TTM-N$(Me)_2$ under 365 nm UV lamp irradiation.

favorable fluorescence characteristics.

3.3. Photostability

The stability of luminescent organic radicals represents a critical parameter in their practical applications. Our initial focus was on investigating the thermal stability of TTM-Br, TTM-NO_2, and TTM-N$(Me)_2$ radicals using thermogravimetric analysis (TGA). The data in Supporting Information S3 reveals that the decomposition temperatures for TTM-Br, TTM-NO_2, and TTM-N$(Me)_2$, corresponding to a 5% mass loss, exceed 246 °C. This level of thermal stability is comparable to that of most closed-shell organic molecules.

Next, we examined the photostability of TTM-Br, TTM-NO_2, and protonated TTM-N$(Me)_2$ radical (TTM-N$(Me)_2$+H) in comparison to TTM. Initially, we exposed cyclohexane solutions of TTM, TTM-Br, TTM-NO_2, and protonated TTM-N$(Me)_2$ (TTM-N$(Me)_2$+H) to identical instrument settings and measured their photoluminescence (PL) spectra. As depicted in Fig. 4a, TTM-Br exhibited slightly better photostability than TTM. Remarkably, TTM-NO_2 and protonated TTM-N$(Me)_2$ (TTM-N$(Me)_2$+H) demonstrated 2 and 3.6 times higher photostability, respectively, compared to TTM. Intriguingly, we observed that TTM-N$(Me)_2$ exhibited exceptional photostability under continuous UV light irradiation.

To assess the photostability of TTM-N$(Me)_2$, we exposed cyclohexane solutions of TTM-NO_2, TTM-Br, protonated TTM-N$(Me)_2$ (TTM-N$(Me)_2$+H) and TTM-N$(Me)_2$ at the same concentration and measured the 375 nm-centered absorbance spectra after irradiation with a 365 nm UV lamp, and compared with TTM. As depicted in Fig. 4b, the half-life of TTM-NO_2, TTM-Br, protonated TTM-N$(Me)_2$ (TTM-N$(Me)_2$+H) and TTM-N$(Me)_2$ was 63, 58, 120 and 6.39×10^5 s, respectively. Clearly, TTM-N$(Me)_2$ exhibited photostability 10,475 times higher than TTM. This remarkable enhancement can be found in most of the donor-acceptor (D-A) type radicals. However, the UV-irradiated photostability of the radical TTM-NO_2 and TTM-Br almost kept same level with TTM, but protonated TTM-N$(Me)_2$ (TTM-N$(Me)_2$+H) showed two times higher photostability than that of TTM.

4. Conclusion

In summary, we have successfully synthesized three novel *meta*-substituted TTM-type radicals, namely TTM-NO_2, TTM-Br, and TTM-N$(Me)_2$, and conducted a comprehensive investigation into their photophysical properties. Our findings indicate that the introduction of -Br has minimal impact on the photophysical properties of TTM, whereas the electron-withdrawing group –NO_2 significantly influences the photostability and Φ_{PL} of TTM. More remarkably, the non-conjugated donor –N$(Me)_2$ at the meta position of TTM greatly enhances the photostability of the TTM-N$(Me)_2$ radical and induces proton-dependent fluorescence. Quantum chemistry calculations and photophysical property investigations have demonstrated that the incorporation of the –N$(Me)_2$ group results in a photostability 10,475 times higher than that of TTM. Furthermore, the protonated state of TTM-N$(Me)_2$ (TTM-N$(Me)_2$+H) exhibits fluorescence activation and 3.6 times greater photostability compared to TTM. These unique properties of the TTM-N$(Me)_2$ radical can be attributed from its D-A properties. Our studies provide valuable insights into the synthesis and further comprehension of *meta*-subtituted TTM-type radicals, paving the way for the exploration of asymmetric *meta*-substituted TTM radicals.

CRediT authorship contribution statement

Ablikim Obolda: Supervision, Validation, Visualization, Writing – original draft, Writing – review & editing, Conceptualization, Formal analysis, Funding acquisition, Investigation, Methodology, Project administration. **Wei Li:** Data curation, Investigation. **Zhaoze Ding:** Formal analysis, Data curation, Investigation. **Fudong Ma:** Data curation, Investigation, Writing – original draft. **Mehrigul Abdulahat:** Formal analysis, Investigation. **Zhuoyang Hu:** Data curation, Methodology. **Jinquan Wang:** Formal analysis, Writing – review & editing.

Declaration of competing interest

The authors declare that the research was conducted in the absence of any commercial or financial relationships that could be construed as a potential conflict of interest.

Data availability

Data will be made available on request.

Acknowledgements

We are grateful for financial support from the National Natural Science Foundation of China (Grant Nos. 21965036 and 21564015), High-level Talent Program of Xinjiang, China Postdoctoral Science Foundation Project (No. 2021MD703886). The authors thank Haoqing Guo from Peaking University for his helping for the DFT calculations.

Appendix A. Supplementary data

Supplementary data to this article can be found online at https://doi.org/10.1016/j.dyepig.2024.112116.

References

[1] Murto P, Bronstein H. Electro-optical π-radicals: design advances, applications and future perspectives. J Mater Chem C 2022;10(19):7368–403.
[2] Huo GF, Shi XL, Tu Q, Hu YX, Wu GY, Yin GQ, et al. Radical-induced hierarchical self-assembly involving supramolecular coordination complexes in both solution and solid states. J Am Chem Soc 2019;141(40):16014–23.

[3] Bejarano F, Olavarria-Contreras IJ, Droghetti A, Rungger I, Rudnev A, Gutiérrez D, et al. Robust organic radical molecular junctions using acetylene terminated groups for C–Au bond formation. J Am Chem Soc 2018;140(5):1691–6.
[4] Sanvito S. Molecular spintronics. Chem Soc Rev 2011;40(6).
[5] Deumal M, Vela S, Fumanal M, Ribas-Arino J, Novoa JJ. Insights into the magnetism and phase transitions of organic radical-based materials. J Mater Chem C 2021;9(33):10624–46.
[6] Tatiana Makarova FP, editor. Carbon-based magnetism:an overview of the magnetism of metal free carbon-based compounds and materials; 2006.
[7] Nguyen TP, Easley AD, Kang N, Khan S, Lim S-M, Rezenom YH, et al. Polypeptide organic radical batteries. Nature 2021;593(7857):61–6.
[8] Bhosale ME, Chae S, Kim JM, Choi J-Y. Organic small molecules and polymers as an electrode material for rechargeable lithium ion batteries. J Mater Chem A 2018;6(41):19885–911.
[9] Tang B, Li W-L, Chang Y, Yuan B, Wu Y, Zhang M-T, et al. A supramolecular radical dimer: high-efficiency NIR-II photothermal conversion and therapy. Angew Chem Int Ed 2019;58(43):15526–31.
[10] Wei P, Oh JH, Dong G, Bao Z. Use of a 1H-benzoimidazole derivative as an n-type dopant and to enable air-stable solution-processed n-channel organic thin-film transistors. J Am Chem Soc 2010;132(26):8852–3.
[11] Ai X, Evans EW, Dong S, Gillett AJ, Guo H, Chen Y, et al. Efficient radical-based light-emitting diodes with doublet emission. Nature 2018;563(7732):536–40.
[12] Murto P, Bronstein H. Electro-optical pi-radicals: design advances, applications and future perspectives. J Mater Chem C 2022;10(19):7368–403.
[13] Peng Q, Obolda A, Zhang M, Li F. Organic light-emitting diodes using a neutral π radical as emitter: the emission from a doublet. Angew Chem Int Ed 2015;54(24):7091–5.
[14] An K, Xie G, Gong S, Chen Z, Zhou X, Ni F, et al. Monoradically luminescent polymers by a super acid-catalyzed polymerization and deep-red electroluminescence. Sci China Chem 2020;63(9):1214–20.
[15] Ballester M, Riera-Figueras J, Castaner J, Badfa C, Monso JM. Inert carbon free radicals. I. Perchlorodiphenylmethyl and perchlorotriphenylmethyl radical series. J Am Chem Soc 1971;93(9):2215–25.
[16] Carilla J, Fajarí L, Juliá L, Riera J, Viadel L. Two functionalized free radicals of the tris(2,4,6-trichlorophenyl)methyl radical series. Synthesis, stability and EPR analysis. Tetrahedron Lett 1994;35(35):6529–32.
[17] Hattori Y, Kusamoto T, Nishihara H. Luminescence, stability, and proton response of an open-shell (3, 5-Dichloro-4-pyridyl) bis (2, 4, 6-trichlorophenyl) methyl radical. Angew Chem Int Ed 2014;53(44):11845–8.
[18] Ai X, Chen Y, Feng Y, Li F. A stable room-temperature luminescent biphenylmethyl radical. Angew Chem Int Ed 2018;57(11):2869–73.
[19] Abdurahman A, Chen Y, Ai X, Ablikim O, Gao Y, Dong S, et al. A pure red luminescent β-carboline-substituted biphenylmethyl radical: photophysics, stability and OLEDs. J Mater Chem C 2018;6(42):11248–54.
[20] Kimura S, Matsuoka R, Kimura S, Nishihara H, Kusamoto T. Radical-based coordination polymers as a platform for magnetoluminescence. J Am Chem Soc 2021;143(15):5610–5.
[21] Kimura S, Kimura S, Kato K, Teki Y, Nishihara H, Kusamoto T. A ground-state-dominated magnetic field effect on the luminescence of stable organic radicals. Chem Sci 2021;12(6):2025–9.
[22] Hattori Y, Kusamoto T, Nishihara H. Enhanced luminescent properties of an open-shell (3,5-Dichloro-4pyridyl)bis(2,4,6-trichlorophenyl)methyl radical by coordination to gold. Angew Chem Int Ed 2015;127(12):3802–5.
[23] Velasco D, Castellanos S, López M, López-Calahorra F, Brillas E, Juliá L. Red organic light-emitting radical adducts of carbazole and tris(2,4,6-trichlorotriphenyl)methyl radical that exhibit high thermal stability and electrochemical amphotericity. J Org Chem 2007;72(20):7523–32.
[24] Gilabert A, Fajarí L, Sirés I, Reig M, Brillas E, Velasco D, et al. Twisted intramolecular charge transfer in a carbazole-based chromophore: the stable [(4-N-carbazolyl)-2, 3, 5, 6-tetrachlorophenyl] bis (2, 3, 5, 6-tetrachlorophenyl) methyl radical. New J Chem 2017;2017(41):8422–30.
[25] Abdurahman A, Hele TJH, Gu Q, Zhang J, Peng Q, Zhang M, et al. Understanding the luminescent nature of organic radicals for efficient doublet emitters and pure-red light-emitting diodes. Nat Mater 2020;19(11):1224–9.
[26] Rozantsev VDSa EG. Advances in the chemistry of stable hydrocarbon radicals. Russ Chem Rev 1973;42(12):1011–9.
[27] Hattori Y, Tsubaki S, Matsuoka R, Kusamoto T, Nishihara H, Uchida K. Expansion of photostable luminescent radicals by meta-substitution. Chem Asian J 2021;16(17):2538–44.
[28] Mattiello S, Hattori Y, Kitajima R, Matsuoka R, Kusamoto T, Uchida K, et al. Enhancement of fluorescence and photostability of luminescent radicals by quadruple addition of phenyl groups. J Mater Chem C 2022;10(40):15028–34.
[29] Hudson JM, Hele TJH, Evans EW. Efficient light-emitting diodes from organic radicals with doublet emission. J Appl Phys 2021;129(18):180901.
[30] Zeng J, Qiu SB, Zhao YJ, Yang XB, Yao Y. Quantum dynamics simulation of doublet excitation and magnetic field effect in neutral radical materials. J Phys Chem Lett 2020;11(4):1194–8.
[31] Akira T, Shun K, Tetsuro K, Moe T, Yasutaka K, Masayoshi N, Hiroshi N. NIR emission and acid-induced intramolecular electron transfer derived from a SOMO−HOMO converted non-Aufbau electronic structure. J Phys Chem 2019;123(7):4417–23.
[32] Proton-induced conversion from non-Aufbau to Aufbau electronic structure of an organic radical with turn-on fluorescence. Chem Res Chin Univ 2022;38(3):798–802.
[33] Gamero V, Velasco D, Latorre S, López-Calahorra F, Brillas E, Juliá L. [4-(N-Carbazolyl)-2, 6-dichlorophenyl] bis (2, 4, 6-trichlorophenyl) methyl radical an efficient red light-emitting paramagnetic molecule. Tetrahedron Lett 2006;47(14):2305–9.